catalysts

MDPI

Article

Influence of 0.25% Indium Addition to Ni/CeO_2 Catalysts for Dry Reforming of Methane

Anita Horváth [1], Andrea Beck [1], Miklós Németh [1], György Sáfrán [2], Matevž Roškarič [3], Gregor Žerjav [3] and Albin Pintar [3,*]

[1] Department of Surface Chemistry and Catalysis, Institute for Energy Security and Environmental Safety, HUN-REN Centre for Energy Research, Konkoly-Thege M. Street 29-33, H-1121 Budapest, Hungary; horvath.anita@ek.hun-ren.hu (A.H.); beck.andrea@ek.hun-ren.hu (A.B.); nemeth.miklos@ek.hun-ren.hu (M.N.)

[2] Thin Film Physics Department, Institute of Technical Physics and Materials Science, HUN-REN Centre for Energy Research, Konkoly-Thege M. Street 29-33, H-1121 Budapest, Hungary; safran.gyorgy@ek.hun-ren.hu

[3] Department of Inorganic Chemistry and Technology, National Institute of Chemistry, Hajdrihova 19, SI-1001 Ljubljana, Slovenia; matevz.roskaric@ki.si (M.R.); gregor.zerjav@ki.si (G.Ž.)

* Correspondence: albin.pintar@ki.si; Tel.: +386-1-47-60-237

Abstract: In this study, the surface and textural properties as well as the catalytic performance of Ni/CeO_2 and NiIn/CeO_2 catalysts prepared by wet impregnation (WI) and deposition–precipitation (DP) are investigated. The addition of Ni (3.0 wt.%) resulted in a decrease in the specific surface area and pore volume in the case of the WI method, possibly due to a blockage of mesopores. A minimal addition of In (0.25 wt.%) caused a further decrease in the surface area in both cases. XRD analysis showed that Ni deposited on CeO_2 by DP resulted in some lattice incorporation, affecting the crystallinity of the support. The H_2-TPR profiles altered depending on the different ways of Ni and In introduction. STEM-EDS-derived elemental maps indicated that the Ni and NiIn particles deposited on CeO_2 using the DP method were somewhat smaller than in the WI synthesis. A comprehensive CO-DRIFTS analysis proved a direct Ni-In interaction in bimetallic samples, leading to the formation of a surface NiIn alloy. Ni/CeO_2 catalysts showed a higher activity in the process of dry reforming of methane (DRM) than the bimetallic counterparts at 650 °C, with the Ni_DP sample performing slightly better. However, the Ni_DP catalyst showed significant coking, which was drastically reduced by the addition of In. The agglomeration of Ni and/or NiIn particles during the 6 h DRM reaction somewhat impaired the catalyst performance. Overall, this study highlights the intricate relationship between the catalyst preparation, surface properties and catalytic performance in the DRM reaction and emphasizes the beneficial role of In addition in reducing the coking of the monometallic catalyst and the critical location and surface morphology of nickel nanoparticles decorated with indium and in contact with ceria.

Keywords: dry reforming of methane; bimetallic catalysts; In-Ni/CeO_2; heterogeneous catalysis; CO_2 utilization

Citation: Horváth, A.; Beck, A.; Németh, M.; Sáfrán, G.; Roškarič, M.; Žerjav, G.; Pintar, A. Influence of 0.25% Indium Addition to Ni/CeO_2 Catalysts for Dry Reforming of Methane. *Catalysts* **2024**, *14*, 383. https://doi.org/10.3390/catal14060383

Academic Editor: Avelina García-García

Received: 10 May 2024
Revised: 5 June 2024
Accepted: 12 June 2024
Published: 15 June 2024

1. Introduction

Global emissions of greenhouse gases such as methane (CH_4) and carbon dioxide (CO_2) are major contributors to climate change, such as global warming, sea level rise, the disruption of agricultural production, etc. [1]. In addition, the production of greenhouse gases has been steadily increasing for years, reaching a level of 54 Gt CO_2 in 2020 according to the UNEP Emission Gap Report 2022 [2,3]. An additional problem with CH_4 production is that CH_4 has a global warming potential 28 times higher than CO_2 over a period of 100 years [4]. Therefore, it is important to convert CH_4 and CO_2 into other gases to mitigate their harmful effects on the environment. By converting these greenhouse gases into less

detrimental forms or useful products, we can effectively reduce their impact on climate change and use them in a more sustainable way.

Dry reforming of methane (DRM) is an important process for converting CH_4 and CO_2 into syngas, a mixture of carbon monoxide (CO) and hydrogen (H_2). This process is a valuable strategy for reducing greenhouse gas emissions and producing syngas that can be reused as a feedstock for various chemicals and fuels. However, the temperature, pressure and catalyst properties must be precisely controlled to achieve optimal conversion, selectivity and lifetime. In addition, the loading of active metal and the chosen carrier influence the conversion of the two gases [5].

Cerium dioxide (CeO_2) and nickel (Ni) are two components commonly used as catalysts for DRM. CeO_2 offers a high oxygen storage capacity and redox properties that enable efficient oxygen transfer during the reaction. Ni, on the other hand, exhibits excellent catalytic activity and promotes the desired reaction kinetics [5]. These properties are crucial, as CeO_2 is used for the activation of CO_2, and Ni sites are used for the activation of CH_4 and also CO_2. Therefore, the Ni/CeO_2 system is favourable for syngas production. However, it also has some disadvantages, such as susceptibility to coke formation due to its high activity, which can lead to catalyst deactivation [6]. In addition, other side reactions can take place that reduce the selectivity of the catalyst for syngas production [5]. Various strategies can be explored to improve this catalyst, such as modifying the catalyst surface, optimizing the catalyst composition and controlling the reaction conditions. These approaches aim to increase the coke resistance, improve the performance of the catalyst and extend its lifetime. One way to reduce coke formation is to vary the activity of Ni for CH_4 dissociation or to increase CO_2 activation. The addition of other metals such as Rh, Ru, Pd, etc., can reduce coke formation by reducing CH_4 activation or activating other mechanisms. However, these precious metals are expensive and are not suitable for large-scale application [5]. On the other hand, indium (In) can be a cheaper alternative to reduce coke formation. This effect was proven in the case of NiIn on SiO_2 [7–9], Al_2O_3 and Ce-promoted Al_2O_3 supports [10,11] in our laboratory. Catalyst coking was eliminated by 2 wt.% indium on a Ni/SiO_2 dry reforming catalyst [7], because indium formed an alloy with nickel, which resulted in a decreased methane decomposition rate, increased hydrogen retention on the surface [8] and reduced CO dissociation [9]. Based on DRIFTS studies, it was suggested that In oxidized by CO_2 or the by-product H_2O formed In_xO_y on NiIn particles, which could act as a reducible oxide, providing active oxygen for the gasification of CH_x species [9]. Simultaneously with the decrease of indium loading to a significantly low promoter level of 0.3 wt.% (Ni/In atomic ratio = 24), the unreducible support was changed for an 8% CeO_2/Al_2O_3 mixed support, and along with the original deposition-precipitation, a simple impregnation method was used for the catalyst preparation [10,11]. Depending on the synthesis route, the beneficial effects of indium promotion were already observable in short TOS experiments [10] or in long stability tests only [11]. CO-DRIFTS measurements with an unusual CO desorption tendency undoubtedly proved the existence of a surface or bulk NiIn alloy that changed its composition, electron density or morphology during a temperature increase. However, an extended metal–ceria interface played a crucial role in the reduction of catalyst coking as well. We should point out that In has a large number of electrons and can be incorporated into CeO_2 due to its similar ionic radius, which increases the concentration of oxygen vacancies [12], and In can increase the metal dispersion, as was observed for In-promoted Cu/CeO_2 in CO_2 hydrogenation [13].

In the present work, we wished to form the simplest Ni-CeO_2 interface, where bulk CeO_2 is the only support compound, and introduce In into the Ni/CeO_2 catalyst in order to reduce possible coke formation using deposition–precipitation or the impregnation synthesis method. In addition, the effect of this 0.25 wt.% In on the catalyst morphology and on the Ni-CeO_2 interaction specifically was investigated using various surface sensitive techniques as well as carbon monoxide-assisted DRIFTS measurements. The limitations of the double role of In as a ceria modifier and metal promoter are discussed. The knowledge

gained in this research provides valuable information for the overall goal of developing clean and efficient technologies to convert greenhouse gases and mitigate climate change.

2. Results and Discussion

2.1. Surface and Textural Analyses

The isotherms of nitrogen physisorption in Figure S1a show that all catalysts exhibit a type IVa isotherm with an H3 hysteresis loop, indicating a mesoporous structure with slit-shaped pores. Moreover, the WI-based samples show a superposition of H3 with an H4 loop given by non-rigid aggregates of platelet-shaped particles with a network of macropores not completely filled with pore condensate [14]. From Table 1, it can be seen that the addition of Ni on the CeO_2 support decreases the specific surface area (S_{BET}) and pore volume, probably due to the pore blocking by Ni [15,16]. In addition, the WI synthesis procedure decreases the S_{BET} to a greater extent than the DP preparation method, which may indicate a higher potential for pore blockage and more aggregated particles than in the case of the DP-based samples. The possible growth of CeO_2 particles is also suggested by the changes in the pore size distributions (Figure S1b). Consequently, the catalytic activity is likely to be lower for WI-based samples than for DP-based solids, as a higher S_{BET} increases oxygen mobility and vacancy formation, which can play a role in CO_2 activation [17]. Interestingly, the minimal addition of In to the Ni/CeO_2 catalysts leads to a further decrease in the S_{BET} and pore volume. This could indicate that the addition of In promotes the mobility and particle growth of CeO_2. A similar surface area decrease caused by the presence of 3.7% In in a $InCu/CeO_2$ impregnated catalyst was observed by Li et al. [18] as well.

Table 1. Determined values of specific surface area (S_{BET}), pore volume (V_{pore}) and average pore diameter (d_{pore}) as well as H_2 consumption (40–650 °C) for the catalysts investigated.

Sample	S_{BET}	V_{pore}	d_{pore}	H_2 Consumed
	m^2/g	cm^3/g	nm	$(cm^3\ H_2)/g_{cat}$
CeO_2	74	0.29	16.7	5.8
Ni_WI	51	0.14	10.9	19.8
NiIn_WI	38	0.13	13.8	18.7
Ni_DP	71	0.25	13.9	20.3
NiIn_DP	64	0.24	14.7	20.1
Ni theoretical	/	/	/	11.5
In theoretical	/	/	/	0.7

To further investigate the phase composition and crystallite size, we performed an XRD analysis on the calcined samples. From the diffractograms in Figure S1c, all samples show characteristic diffractions for cubic Fm-3m CeO_2 corresponding to PDF ICDD 01-080-6915 (a = 0.541 nm), except for the Ni_DP sample, where the diffractions correspond to PDF ICDD 04-015-0377 (a = 0.540 nm). For all catalysts, the characteristic peak that dominates the diffractograms is at 28.5° (111), followed by peaks at 47.5° (220) and 56.4° (311). In all XRD patterns, the peaks of Ni oxide and In oxide are absent, indicating that they are highly dispersed and small. However, comparing the peak positions of the samples in Table 2, the CeO_2 (111) and (220) peaks of the Ni_DP sample shifted to higher values compared to the other catalyst samples and the pure CeO_2. Presumably, during the calcination at 650 °C, a strong interaction occurred between NiO and CeO_2, resulting in Ni incorporation into the supporting oxide. Interestingly, in the bimetallic NiIn_DP sample, such a shift could not be observed, as In would have hindered the Ni inclusion, resulting in an ordinary CeO_2 peak position and cell parameters (Table S1), as was observed in case of both catalysts prepared using wet impregnation synthesis. This suggests that in the NiIn_DP sample and both WI catalysts, the extent of Ni inclusion into the CeO_2 lattice is limited, and Ni and In oxides should be located on the surface of ceria [12]. The crystallite sizes of CeO_2 determined from the most intense reflections are also presented in Table 2. Based on these, we can deduce that

the addition of Ni using the WI preparation method only slightly decreases the crystallinity of CeO_2, but the DP synthesis procedure does to a greater extent. This is probably due to the deposition–precipitation method with urea as the precipitant, leading to a more intense metal-support interaction and the disruption of pure CeO_2 domains by Ni cations. The addition of In improved the crystallinity and increased the crystallite size in both cases compared to the monometallic samples, which could be due to the aforementioned effect of In attenuating the decrease of crystallinity in CeO_2 particles (Table 2) and the hindrance of Ni incorporation.

Table 2. Estimated crystallite sizes of CeO_2 at 28°, 47° and 56° according to the Scherrer equation for spherical particles, and peak positions for (111), (220) and (311) crystal planes of samples in the calcined state.

Sample	@28°	@47°	@56°	(111)	(220)	(311)
		nm			°	
CeO_2	31.3	27.01	29.1	28.55	47.49	56.44
Ni_WI	28.5	26.6	26.4	28.56	47.50	56.35
NiIn_WI	30.3	29.6	29.9	28.56	47.49	56.35
Ni_DP	21.5	21.1	22.2	28.65	47.57	56.43
NiIn_DP	25.7	25.5	27.1	28.54	47.48	56.33

Next, we performed a temperature-programmed reduction (TPR) with H_2 to obtain information about the reducibility of the oxide components and the metal-support interactions. All the TPR profiles shown in Figure 1 were quantified concerning the exact H_2 consumption of the catalysts. Since the samples contain CeO_2, the redox change from surface/subsurface Ce^{4+} to Ce^{3+} along with the NiO reduction were expected to be observed simultaneously. Indeed, the calculated H_2 consumption values in Table 1 are always higher than what the corresponding Ni and In content could result in. This means that a partial reduction of CeO_2 happens as well. It can be seen that the DP-based samples have a slightly higher H_2 consumption than the WI-based samples. Moreover, the H_2 consumption is slightly reduced by the addition of In compared to the monometallic Ni samples. This could indicate that In interacts with Ni particles and thereby alters the MSI and, thus, the reducibility of the samples. The TPR curves in Figure 1 exhibit two main peaks: there is always a smaller peak well below 300 °C and a larger main peak around or above that temperature, depending on the sample. The first peak is extremely sharp in the case of the DP samples. We assign these peaks to the reduction of small NiO clusters almost atomically dispersed in/on the ceria matrix and to the reduction of adsorbed oxygen species at CeO_2 vacancies [19,20]. These vacancies are formed because of the Ni^{2+} incorporation into the CeO_2 lattice, which generates a charge imbalance. The larger peaks assignable to the reduction of NiO with different degrees of metal-support interaction spread up to 425–450 °C. Although XRD detected a strained CeO_2 structure for the Ni_DP sample, the reduction properties of the In-containing counterpart differed only by a small shift in the peak positions for higher temperatures, but the shapes of the curves were almost identical. This would imply that nickel and indium oxide species are located at different places and do not form an alloy, as was reported for a similarly prepared CuIn/CeO_2 catalyst sample [18].

Among the WI samples, there was a larger difference caused by the presence of indium. The trend was the same: the peaks shifted with 20–30 °C to higher temperatures, suggesting an increased interaction or even particle size differences [21,22]. This could indicate that In improves the MSI compared to the monometallic WI sample, but the sharpness of the first peak disappeared, suggesting a different distribution of NiO in the NiIn_WI catalyst and the presence of less oxygen vacancies. We should note that for the NiIn_DP and NiIn_WI samples, an additional low intensity peak can be observed at lower temperatures (at 134 or 161 °C) that might be assigned to the reduction of surface NiO-InO_x species.

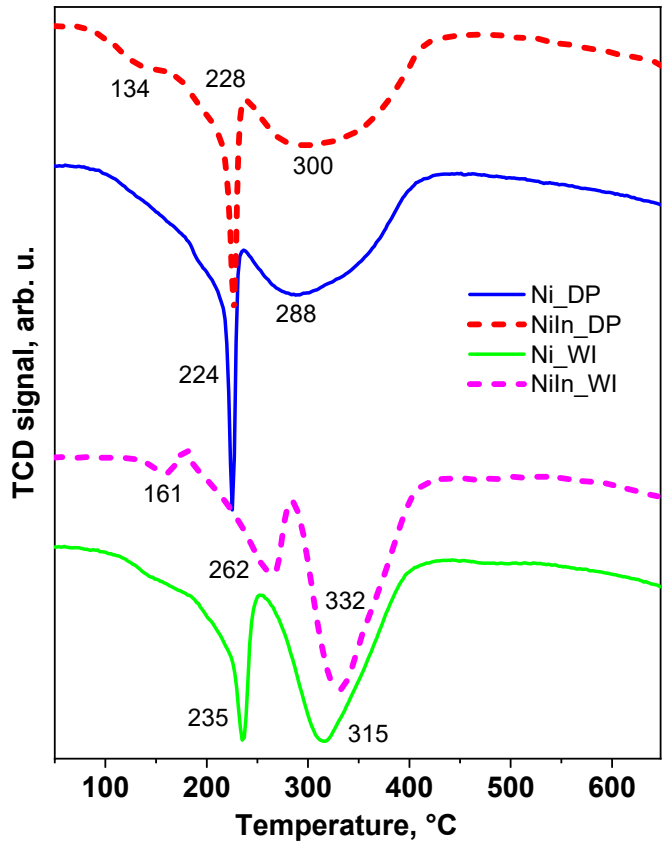

Figure 1. H_2-TPR profiles of the investigated nanosolids.

The morphological properties and elemental compositions of the catalysts were further investigated using TEM, STEM-EDS and SEM-EDS analyses. Unfortunately, the Ni particles cannot be recognized in the TEM images of the CeO_2-supported Ni and NiIn catalysts based on their contrast or shape. In most cases, the dark spots in the TEM images (or the white spots in the HAADF images), which were assumed to be metallic particles, were only ceria, as shown by the Ni maps obtained during the STEM-EDS measurements (Figures S2 and S3). Therefore, we could not determine the mean particle size and distribution from the TEM images. However, an indication of metal dispersion from the elemental maps could be obtained, as shown for the calcined and reduced (fresh) samples in Figure 2. With the exception of the NiIn_WI sample, Ni exhibits a relatively high dispersion (shown in yellow in the Ni maps, Figure 2). In the Ni_DP sample, in addition to larger Ni particles between 2–8 nm, numerous very small Ni particles or clusters are distributed over the cerium dioxide, which presumably interact strongly with the support. They probably originate from the reduction of Ni^{2+} dissolved in CeO_2 during calcination [23]. The Ni particles in the NiIn_DP sample appear to be rather spherical, with diameters between 3–7 nm. The Ni particles in the Ni_WI sample are between 3–7 nm, with one particle of 20 nm size, while much larger particles up to 45 nm are also present in the NiIn_WI catalyst along with the smaller ones around 14 nm. The Ni/In ratios over the entire measured area of the fresh NiIn_DP and NiIn_WI samples were found to be 38 and 27, respectively (Figure 2). The low In concentration leads to apparent intensity lines (arising from noise) in the ED spectra only when accumulated over such large areas. The In maps (shown in red in Figure 2c,d) show no clear aggregation of indium. Previously, for pure alumina and CeO_2-promoted alumina supported NiIn catalysts with the same Ni and In loadings, it was deduced that In was enriched in/around Ni particles, although a smaller fraction was on the support as well [10]. Here, in the CeO_2-supported analogs, the In concentration (In/Ce) could not be measured and compared on smaller Ni-rich and Ni-poor surfaces due to the low signal intensity. Accordingly, we assume that most of the In in the NiIn/CeO_2 catalysts

prepared by DP and WI methods are uniformly distributed over the catalyst surface and present in both Ni and the ceria components. Li et al. [18] observed on the STEM-EDX elemental maps of a Cu5In5/CeO_2 sample that Cu and In signals were not overlapped and deduced that separated Cu and In species were present on CeO_2. This also agrees with our results, but the metal content in our case strongly limits the confidence.

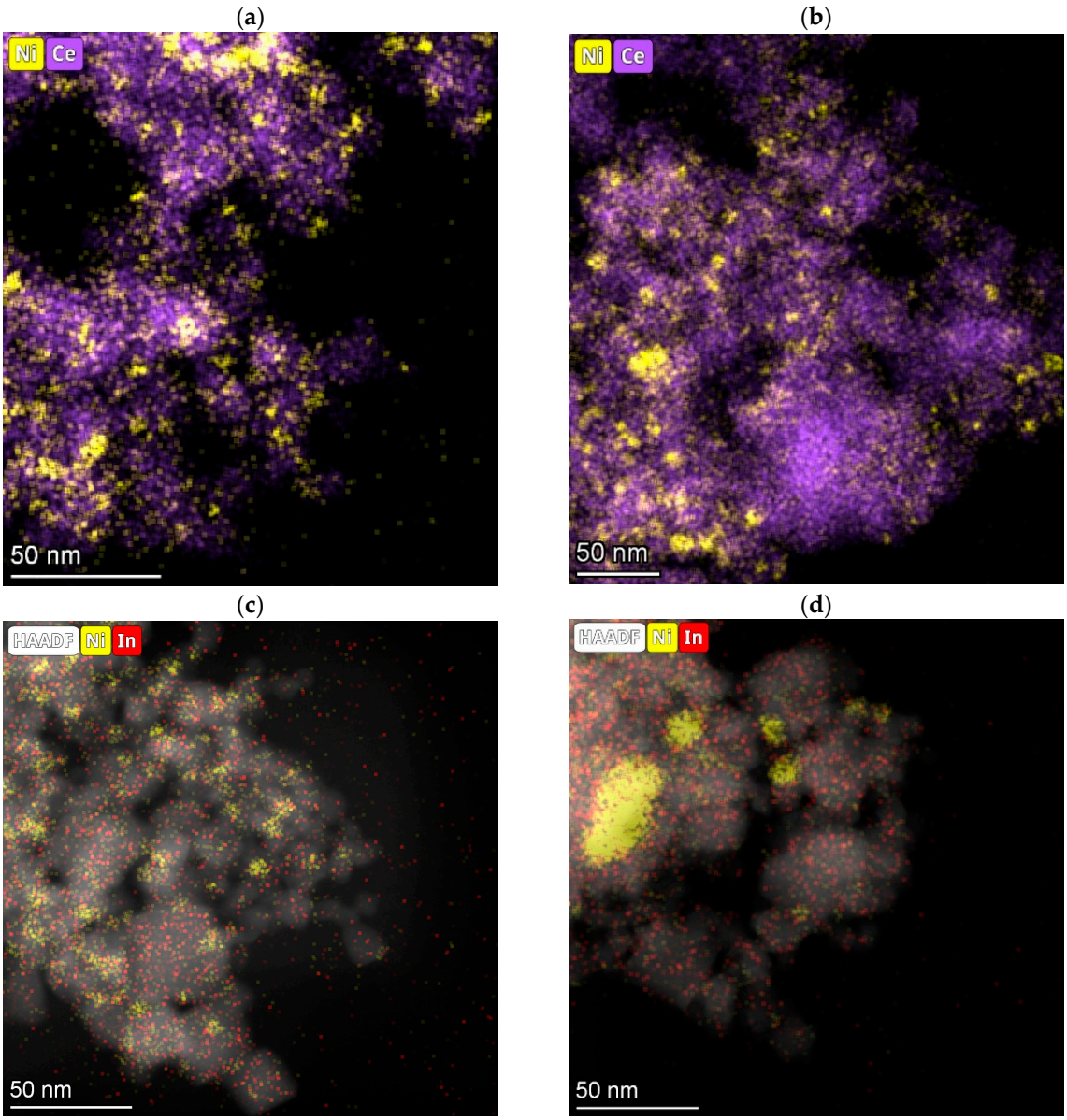

Figure 2. Elemental maps of calcined/reduced (fresh) (**a**) Ni_DP, (**b**) Ni_WI, (**c**) NiIn_DP and (**d**) NiIn_WI catalysts. The Ni/In atomic ratios on the measured areas of NiIn_DP and NiIn_WI samples are 38 and 27, respectively.

Our results from the SEM-EDS analysis of the catalysts under study (shown in Figure S4 and Table S2) indicate the good distribution of Ni and In in the samples and that the actual loading of In and Ni is consistent with the nominal one.

The surface concentrations and oxidation states of the catalyst components were analyzed using the XPS method. Table 3 collects the most important results of this measurement, which was conducted after the in situ reduction treatment at 650 °C, and the corresponding Ni 2p and In 3d spectra are shown in Figure S5. The surface concentration of Ni (see Ni/Ce atomic ratio) was higher and equal in the DP samples and lower in the

WI-type ones, but it was extremely small in the NiIn_WI solid. This means, in general, differences in the dispersion or in the location of nickel that can be buried under the ceria/in the pores of the support. Based on the particle sizes estimated using STEM-EDS and the DRIFT spectra of adsorbed CO (discussed later), we suggest that in the Ni_WI catalyst, the metal particles are hidden deeper in the CeO_2 pores than in the DP samples, while in the NiIn_WI sample, they may form larger aggregates as well. As for the oxidation state of Ni, it was ascertained to be metallic, with a binding energy of 852.6 eV (Figure S5). An indium signal was detected in both bimetallic catalysts. It shows that indium must be partially oxidized, as the 444.3 eV BE is somewhat higher than the BE of the metallic state (443.7 eV in [24]) but lower than the oxidized value determined on calcined CeO_2-Al_2O_3-supported catalysts with the same In concentration (444.7 eV in [11]). The small difference obtained in the Ni/In ratios (2.67 for DP; 2.00 for WI) cannot be used for any further reasoning, but the value is definitely far from the theoretical bulk Ni/In = 24 and much lower than in our previous study on an impregnated NiIn/CeO_2-Al_2O_3 catalyst (that gave a surface Ni/In value of ~7). This suggests that In is not accompanied by the metallic nickel but rather is enriched on the surfaces of the catalysts in the oxide matrix. An oxidic state of indium was confirmed inside the CeO_2 matrix (not alloyed with the Cu metal) of an impregnated and reduced 4%Cu3.7%In/CeO_2 catalyst [18]. In contrast, metallic indium was detected in a 1%In5%Cu/CeO_2 catalyst sample prepared using a specific solid phase reaction. It seems that the alloying ability of indium depends on the preparation method and loading as well.

Table 3. Surface atomic ratios and concentrations of surface Ce^{3+} determined from XPS measurements on the reduced catalysts.

Sample	Ni/Ce Ratio	Ni/In Ratio	Ce^{3+} Content of All Surface Ce
			%
Ni_DP	0.030		7
NiIn_DP	0.030	2.67	8
Ni_WI	0.014		4
NiIn_WI	0.006	2.00	10

The ceria component was slightly reduced upon the in situ reduction in all samples. The concentration of Ce^{3+} is only 7–8% for the DP samples and 4% for Ni_WI and 10% for the NiIn_WI counterparts, but we should note that the error of such a calculation is relatively high, since the determination of the Ce^{3+} content is really complicated (see ref. [10] for further details). Keeping this all in mind, it seems that Ni is in a metallic state, but it is presumably partly covered or shaded by CeO_2. This burial of Ni inside the pores is more pronounced in the WI samples, and the lower metal dispersion of the NiIn_WI sample amplifies this. Indium is partially in an oxidic state; that means it is distributed in ceria and not in a bimetallic bulk NiIn alloy. However, it might be present in a zero-oxidation state on the surfaces of the nickel particles. The most reducible surface ceria is present in the NiIn_WI sample. The same surface Ni concentration values and the same ceria reduction degree suggest no influence of indium promotion in the case of the DP preparation method, as it was detected using TPR measurements as well.

2.2. CO-DRIFTS Investigation of Catalysts

As a sensitive and efficient method for surface characterization, CO adsorption followed by infrared spectroscopy was used to compare the electronic and geometrical/morphological states of the surface Ni sites in the different catalysts. It is known that the Ni surface oxidizes rapidly in contact with air at room temperature or at elevated temperatures, even in Ar. Therefore, an additional milder in situ reduction at 500 °C for 30 min in the DRIFTS cell was performed before the chemisorption experiments, after the standard ex situ reduction at 650 °C, to obtain the same catalyst surface and Ni state that was tested in the DRM reaction. CO adsorption at different Ni sites on the surface shows

different CO stretching vibration bands. The linearly adsorbed CO occurs in the range of 2100–2000 cm^{-1}, while the bridging CO (Ni_2CO) and the multi-coordinated CO (Ni_3CO or Ni_4CO) are found between 1970–1890 cm^{-1} and below 1890 cm^{-1}, respectively [25–27]. The linear carbonyl species are the typical monocarbonyl species on Ni surfaces, which occur between 2065–2040 cm^{-1} (the band frequency increases with a decreasing coordination number of Ni), and the $Ni(CO)_x$ (x = 2, 3) polycarbonyl species (on coordinatively unsaturated Ni sites, corners, edges and kinks), which are detectable at higher wavenumbers around 2080–2070 cm^{-1} [25–27]. The formation of $Ni(CO)_4$ can occur at highly defective Ni atoms of highly dispersed Ni nanoparticles: the Ni atoms split off from the Ni particle, and the $Ni(CO)_4$ physisorbed on the support surface results in a CO band at about 2050 cm^{-1}, which is narrower than that of linear carbonyls [25,27,28].

Figure 3 shows the CO chemisorption spectra recorded in the presence of 1% CO/Ar after a 5 min exposure at room temperature (bands with maxima at 2174 and 2114 cm^{-1} belong to CO in the gas phase). For the monometallic Ni_DP catalyst (blue spectrum), a band with a maximum at 2072 cm^{-1} attributed to some Ni di- or tri-carbonyls, with a distinct sharper peak of $Ni(CO)_4$ species at 2042 cm^{-1} [25], and bands of various bridged and bidentate carbonyls at 1956, 1918 and 1883 cm^{-1} are detected. In the spectrum of the Ni_WI sample (green curve), the contribution of polycarbonyls is lower at high wavenumbers, and no $Ni(CO)_4$ peak is observed. This indicates that the Ni surface of the Ni_WI sample is smoother and has a lower number of defective Ni adatoms. This difference can be caused by the ceria coverage of the small Ni particles of the Ni_DP sample formed by the exsolution of Ni^{2+} ions upon the high temperature reduction, producing a rough, uneven metal surface.

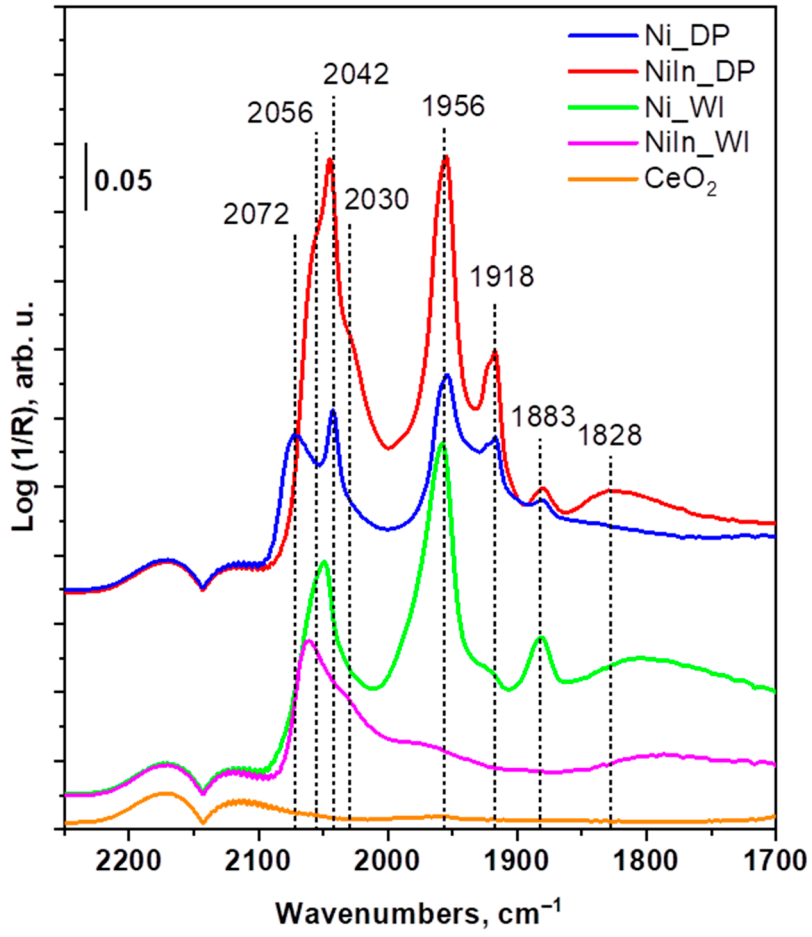

Figure 3. DRIFT spectra of CO adsorption on the catalysts examined at room temperature after 5 min of exposure.

Looking at the CO chemisorption curves of the bimetallic samples (Figure 3), it can be seen that the introduction of indium decreases the overall intensity of the CO band in the case of the WI-based sample, while it is increased in the case of the DP-derived sample. The increase in the total CO band area implies a larger Ni surface area and vice versa, indicating a higher dispersion in the NiIn_DP sample compared to the Ni_DP and NiIn_WI solids, the latter having the lowest dispersion among the samples. The presence of physisorbed $Ni(CO)_4$ can be suspected in the NiIn_DP sample based on the shape of the CO band at 2042 cm^{-1} (red curve), while no sign of $Ni(CO)_4$ can be seen in the NiIn_WI sample (magenta curve), similar to the Ni_WI sample. However, both bimetallic samples also show a shoulder at 2030 cm^{-1}, which can be attributed to linear CO species chemisorbed at Ni sites with In neighbours [9,10]. In addition to this similarity, a striking difference is the sharp decrease in the bridge region in the NiIn_WI sample, which is still present in the bimetallic DP-based sample. Such a decrease in the relative ratio between the bridge and linear CO bands, as observed for the NiIn_WI sample, clearly proves that the smooth, densely packed (111) and (100) Ni surface is strongly diluted by In atoms, reducing the concentration of Ni-Ni neighbours [9,10], so the possibility for adsorbed CO molecules to bond to two adjacent nickel atoms lowered. Such strong masking of the neighbouring Ni atoms by In means that indium must be enriched on the surfaces of the less dispersed Ni particles. This surface enrichment cannot be seen for the NiIn_DP catalyst, probably because it has a smaller particle size and less indium atoms present on nickel (a higher number of Ni atoms on the surface and, thus, a lower possible extent of In coverage).

Figure 4 summarizes the spectra recorded after chemisorption of the CO in 5% H_2/Ar during the temperature-controlled surface desorption/reaction process up to 300 °C. The room temperature spectrum of each samples measured in presence of 1% CO/Ar gas are also added (dashed line). For the Ni_DP sample (Figure 4a), the rapid disappearance of physisorbed $Ni(CO)_4$ was observed by the decreasing band at 2042 cm^{-1}, when CO was purged from the cell at room temperature. This was accompanied by the appearance of new, sharp bands with lower frequencies at 1987, 1931, 1908 and 1879 cm^{-1} for both DP-based samples, which can be assigned to $Ni(CO)_4$ and its derivatives (e.g., tricarbonyl) bound to the ceria surface via one or two CO ligands [27,29,30]. Such surface species have been observed on zeolite and alumina surfaces after the adsorption of $Ni(CO)_4$, for example, as Al^{3+}-$OCNi(CO)_3$ at 2145, 2095 and 1903 cm^{-1} and as Al^{3+}-$OCNi(CO)_2$ at 2065, 1985 and 1835 cm^{-1} [30]. The polycarbonyls visible in the spectrum of the Ni_DP sample with the band at 2070 cm^{-1} are also weakly bound and are eliminated (or transformed) below 100 °C. At higher temperatures, the gradually decreasing linear CO band of the monocarbonyls is red-shifted to 2025 cm^{-1}, the bridging CO band is strongly reduced and red-shifted to 1897 cm^{-1} and the multibonded is red-shifted to 1807 cm^{-1} until all these carbonyls are completely eliminated at 200 °C from the Ni_DP sample.

In the case of the NiIn_DP sample (Figure 4c), the removal of CO from the gas phase at room temperature by switching to a 5% H_2/Ar stream resulted in similar spectral changes as for the Ni_DP sample. The unresolved two-component band at 2049 cm^{-1} decreased slightly, and the bands at 1956 and 1918 cm^{-1} decreased more, while other bands appeared or increased at the same wavenumbers as in the case of the Ni_DP sample (1987, 1908 and 1897 cm^{-1}). The decrease in the linear carbonyl bands upon the removal of CO from the gas phase can be examined in more detail using the difference spectra shown in Figure S6. The decreasing linear CO bands of the DP samples (blue and red curves) are well resolved as a higher frequency band of subcarbonyls (2078 and 2065 cm^{-1} for Ni_DP and NiIn_DP samples, respectively) and a peak of physisorbed $Ni(CO)_4$ at 2042 cm^{-1}. The lower frequency value of the subcarbonyl peak in the NiIn_DP sample could be a sign of Ni-In interaction [9]. After the disappearance of these components from the spectrum of the NiIn_DP catalyst, there was a significant redshift of the remaining linear monocarbonyl CO band to 2030 cm^{-1} up to 150 °C, with no appreciable loss of intensity (Figure 4c), as we had already observed such changes in the NiIn/SiO_2 samples [9]. (It should be recalled that in the monometallic Ni_DP sample, the linear CO bands decreased monotonically

up to 150 °C (Figure 4a)). The CO originating from the decomposition of $Ni(CO)_4$ and its derivatives could form linear monocarbonyls on the Ni sites interacting with neighbouring In on the crystal facets of the NiIn_DP sample, while on the Ni_DP sample, these CO molecules leave the surface due to weaker adsorption or a higher reactivity towards H_2 on the non-disturbed Ni sites. It should be noted that the bridging CO at 1956 cm^{-1} on the NiIn_DP sample decreased sharply up to 150 °C. With a further increase in the temperature, both the linear bands and the much weaker bridging bands gradually decreased and shifted to 2000 and 1920 cm^{-1}, respectively, and they disappeared completely only at 300 °C, i.e., at a temperature 100 °C higher than in the case of the monometallic counterpart. The higher stability of the chemisorbed linear CO species is explained by the presence of In in the form of a surface NiIn alloy, as was deduced in our previous studies [9,10]. The lower frequency of linear CO on the DP-prepared bimetallic sample compared to the monometallic sample (2011 vs. 2025 cm^{-1} at similar coverages, at 200 °C on the NiIn_DP sample and 150 °C on the Ni_DP solid, respectively) can also be attributed to the close presence of Ni and In and the Ni-In interaction.

In the WI-prepared samples (Figure 4b,d), the characteristic band of $Ni(CO)_4$ and its support-bound derivatives in the broad band at 2046 cm^{-1} could not be detected either in the presence of CO or after its removal, nor could it be detected in their difference spectra in Figure S6. In the difference spectrum of the Ni_WI sample (Figure S6), the broad decreasing band (at 2050 cm^{-1}) did not resolve in contrast to the DP-based sample, and its dominant part could rather be assigned to the monocarbonyls bound to low-coordinated Ni sites. In the difference spectrum of the NiIn_WI sample, only one band decreased at 2068 cm^{-1} (polycarbonyl), and no band change can be seen around 2042 cm^{-1}. This indicates the absence of coordinatively highly unsaturated Ni sites on both catalysts. After the removal of CO from the gas phase, the linear and especially the bridging CO band on the Ni_WI sample decreased much faster than on the Ni_DP catalyst (see Figure 4b). This could be the result of the surface reaction of CO in the presence of H_2 via COH formation [30]. (In the Ni_DP sample, the Ni polycarbonyls block the Ni sites, so the platform for such a surface reaction is lower. In addition, the polycarbonyls provide a temporary CO pool that prolongs the lifetime of the adsorbed CO species.) With an increasing temperature, the remaining linear and bridge bands of the Ni_WI sample further decreased and shifted to lower wavenumbers until they completely disappeared at 200 °C, just as for the Ni_DP sample. The bimetallic NiIn_WI catalyst (Figure 4d) shows the same CO desorption profile in the linear CO band range and from 150 °C in the entire CO stretching range as the DP counterpart, but with a significantly lower intensity.

After the temperature ramp in 5% H_2/Ar up to 300 °C, the cleaned Ni(In)/CeO_2 surfaces were again exposed to 1% CO/Ar for 5 min and then rinsed with 5% H_2/Ar for 5 min. The spectra recorded after 1 and 5 min in the presence and absence of CO are shown in Figure 5. After 1 min of contact with CO, all samples showed linear CO bands with maxima at about 2047–2037 cm^{-1} and strongly reduced weak bands below 2000 cm^{-1} in the region of the bridge and the multiple-bond CO. After another 4 min, all bands largely decreased in the case of the monometallic Ni samples. This must be the result of CO decomposition, which produces carbon and surface oxygen (NiO) that poison the Ni sites. In the bimetallic samples, In promotion prevented the decomposition of the adsorbed CO, as the CO band did not change during these 4 min (in the presence of CO gas). The three-times lower intensity of the stable CO bands on the bimetallic WI sample than on the DP-based bimetallic sample indicates a much lower metal dispersion of the NiIn_WI catalyst, but an overall hindered CO dissociation ability for both bimetallic samples. In the absence of CO gas, the CO bands almost completely disappear on the monometallic samples during one minute in the 5% H_2/Ar stream, while this happens gradually on the bimetallic samples, accompanied by a redshift from about 2045 cm^{-1} to 2002 cm^{-1} after 5 min. In the initial spectra of both NiIn samples, the highest frequency component can be assigned to CO bound to Ni atoms with little or no interaction with indium, while the lower frequency component at about 2025 cm^{-1} can be assigned to CO adsorbed on Ni with a

stronger interaction with indium (surrounded by In neighbours), which shifts further with time. The electronic effect of In is thus reflected in the low-frequency stretching vibration of CO adsorbed on Ni, which is perturbed by In [31].

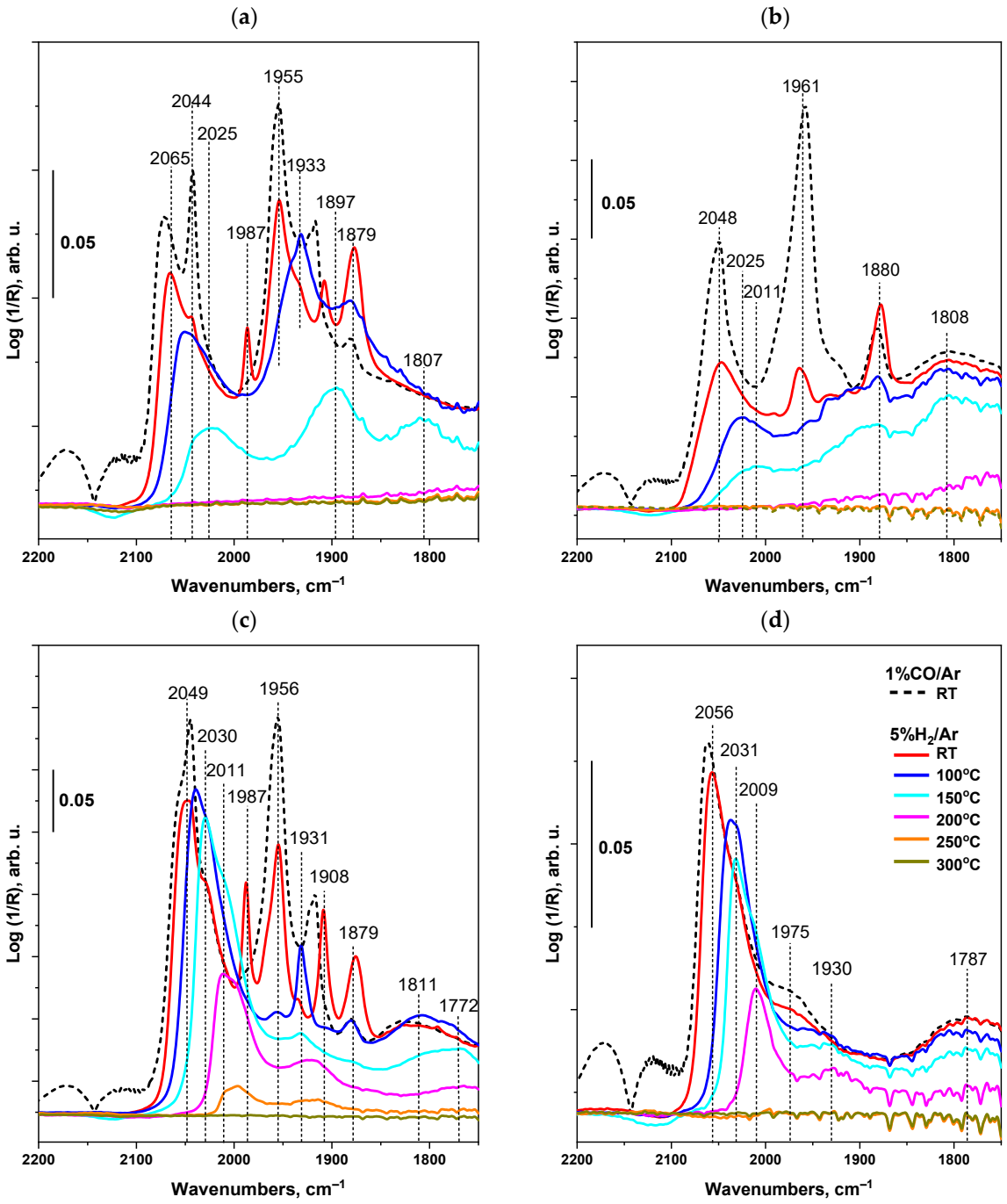

Figure 4. DRIFT spectra of adsorbed CO on (**a**) Ni_DP, (**b**) Ni_WI, (**c**) NiIn_DP and (**d**) NiIn_WI samples measured during a temperature-programmed treatment up to 300 °C in 5% H_2/Ar. The original spectra recorded in 1% CO/Ar are also shown as dotted lines. The temperature legends are the same for all graphs and are shown in panel (**d**).

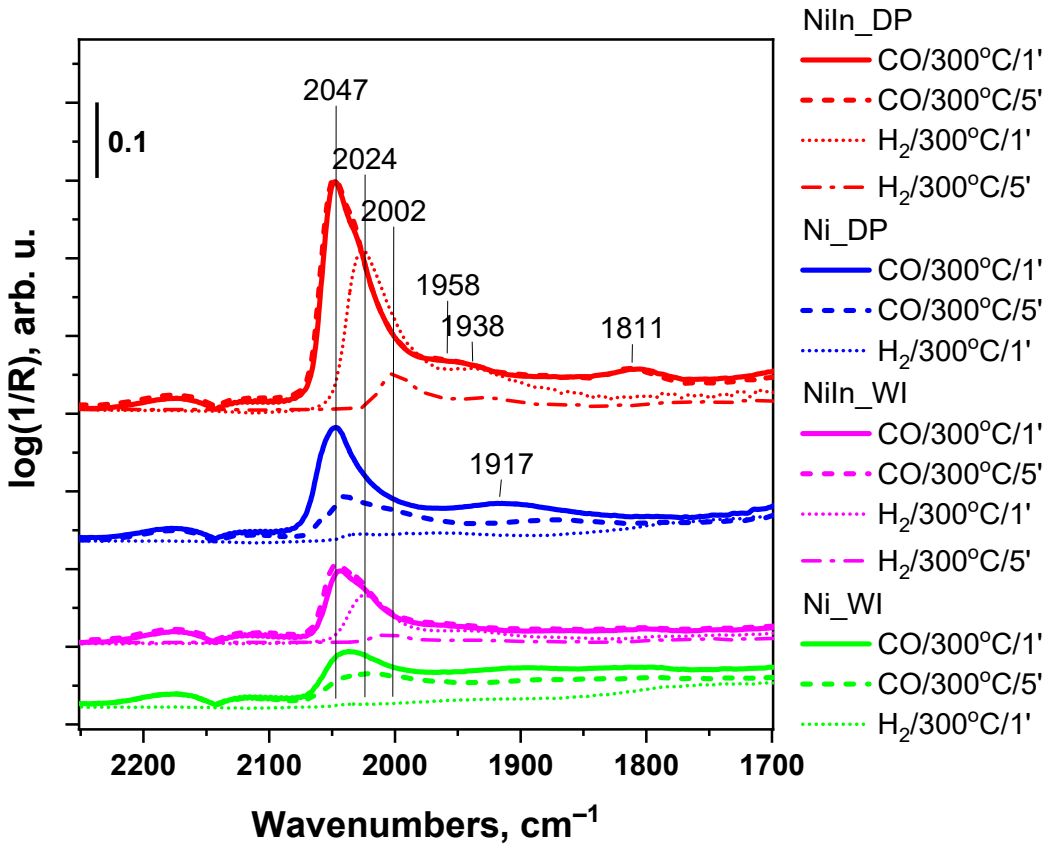

Figure 5. DRIFT spectra of adsorbed CO on the various catalyst samples, measured at 300 °C in 5% CO/Ar after 1 and 5 min, then in 5% H_2/Ar after 1 min and, in the case of the bimetallic samples, also after 5 min.

In summary, the CO-DRIFTS results indicate that the Ni_DP and NiIn_DP samples prepared using the DP method contain highly undercoordinated Ni centers capable of forming Ni tetracarbonyl, whereas the counterparts prepared using the WI method do not. These sites may be located on tiny particles or on larger particles with a rough surface or partially covered by CeO_2 moieties (Note that these strongly undercoordinated Ni atoms of the DP-based samples may be the starting points for CH_4 activation and dissociation during DRM at high temperature and, at the same time, the active sites for coke formation in the case of insufficient coke gasification). In the bimetallic samples, there is a direct interaction between Ni and In, as evidenced by the increased thermal stability of adsorbed CO and the redshift of its stretching vibrational frequency due to the indium-induced electronic perturbation of Ni. The increased ratio of linear-to-bridge CO intensity indicates a dilution of the Ni surface by In (clearly evident in the NiIn_WI sample) and thus the formation of a NiIn (surface) alloy. This In promotion prevented the decomposition of the adsorbed CO at a higher temperature in contrast to the monometallic counterpart in the case of both preparation routes. However, the Ni surface area in the NiIn_WI sample is very low, which is probably due to the presence of larger NiIn particles. The monometallic Ni_WI catalyst adsorbs slightly more CO than the Ni_DP sample, and a significant portion of the adsorbed CO was already eliminated/converted at room temperature in the presence of H_2, suggesting an increased reactivity of the Ni–ceria interface in this sample.

2.3. Catalytic Tests

The results of the DRM catalytic tests carried out at 650 °C and atmospheric pressure in the quartz fixed-bed reactor are shown in Figure 6. It can be seen from Figure 6a,b that in the given range of operating and reaction conditions, the highest conversions of CH_4 and CO_2 were measured on monometallic catalysts followed by their bimetallic

counterparts, but NiIn_WI had negligible activity. The CO_2 conversions were higher than the CH_4 conversions, which is due to the fact that the RWGS reaction occurs simultaneously with the main DRM reaction. For the monometallic catalysts, the Ni_DP sample exhibits a very similar activity compared to the Ni_WI solid, although it contains smaller Ni particles according to the STEM-EDS estimation and has a larger specific surface area (Table 1). The addition of small amounts of In, which clearly dilutes the Ni particles according to the CO-DRIFTS studies, significantly decreases the activity regardless of the catalyst preparation method used. However, of the catalysts studied, the NiIn_DP sample exhibits the highest selectivity towards H_2 and CO (Figure 6c,d). The yields of H_2 and CO obtained with DRM (Figure S7) on the catalysts investigated decrease in the following order: Ni_DP > Ni_WI > NiIn_DP > NiIn_WI, which is consistent with the order of decreasing CH_4 or CO_2 conversions. Furthermore, higher H_2/CO yield ratios were obtained on monometallic Ni catalysts than on their bimetallic NiIn counterparts (Figure 6e); the highest, about 0.4, was obtained in the presence of the Ni_DP catalyst. In our previous work, we obtained similar effects due to the presence of In in different nickel catalysts [7–11]. Indium present on either nickel or distributed in the CeO_2 matrix can facilitate CO_2 activation; this is why the CO_2/CH_4 conversion ratio is always higher for the active In-promoted samples. Moreover, the nickel surface that contains In atoms decreases the CH_4 dissociation. This is why the activity drops for the NiIn_DP sample. The low activity of the NiIn_WI catalyst can be explained by the close to full coverage of smooth planes of nickel particles by indium (remember, almost no bridge CO was formed during CO chemisorption in the DRIFTS experiments) and the least metal dispersion (the lowest surface nickel concentration). Although the only proof for the bimetallic NiIn surface sites was delivered using DRIFTS experiments until now, the catalytic behaviour of the NiIn_DP sample can be considered as another sensitive tool to show the great influence of 0.25 wt.% In loading, from which only a minute amount must be located on nickel but causes differences in the activity and, as we will see in the next section, in catalyst coking as well.

The results listed in Table 4 show that during the DRM reaction, coking of the catalysts prepared using DP occurred, more (5.3 wt.%) in the case of the Ni_DP sample. Importantly, when the Ni particles were diluted with In (NiIn_DP catalyst), the extent of coking was significantly reduced, almost by a factor of 10, while almost no carbonaceous species accumulated on the surfaces of WI-based catalysts. The results of the elemental analysis (Table 4) are in very good agreement with the results of the carbon balance (Figure S8a), which predicts the formation of carbonaceous deposits in the case of Ni_DP and NiIn_DP catalysts. The difference in the behaviours of the catalysts is explained by the increased CH_4 dissociation ability of small, defective metallic Ni sites in the DP samples (which were detected by the tetracarbonyl-forming sites in the CO-DRIFTS experiments) and by the presence of larger Ni and NiIn ensembles in the WI samples surrounded by ceria, allowing for the gasification of carbon to CO. Most of the nickel in the WI-based samples is located in the pores of the support, as the specific surface area was reduced by the impregnation and calcination step (pore filling), and XPS also detected lower nickel concentrations on the surface after reduction (metallic particles were still hidden). The nickel particles are therefore in closer contact with the ceria, which is necessary to prevent carbon deposition, as the surface carbon can react with the mobile oxygen, accompanied by a rapid Ce^{4+}/Ce^{3+} redox step in the vicinity of the nickel. The O vacancy formed can be quickly replenished by CO_2. Note that although the ceria in the Ni_DP sample is supposed to cover part of the rough Ni surface, it is not able to prevent coke deposition due to rapid CH_4 dissociation, as most Ni particles are probably not in the pores of the ceria. Unfortunately, high amount of H_2O must have been formed in all cases because of the oxidation of the surface hydrogen at this relatively low reaction temperature.

The significant coke-reducing effect of indium promotion in the case of NiIn_DP sample is evident and was expected based on our previous findings using different supports [7–11]. This means that even when the CH_4 dissociation is accelerated by the surface properties of small, rough Ni particles, indium can play its role via surface alloy formation

with Ni and decrease the carbon accumulation via decreasing the rate of CH_4 dissociation over this bimetallic NiIn surface while keeping a relatively higher CO_2 conversion. Based on the catalytic phenomena and the results of the DRIFTS experiments, we suggest that the little indium on the surface of nickel starts to accommodate the smooth planes first, because the highly undercoordinated nickel atoms remained free for tetracarbonyl formation and CH_4 dissociation.

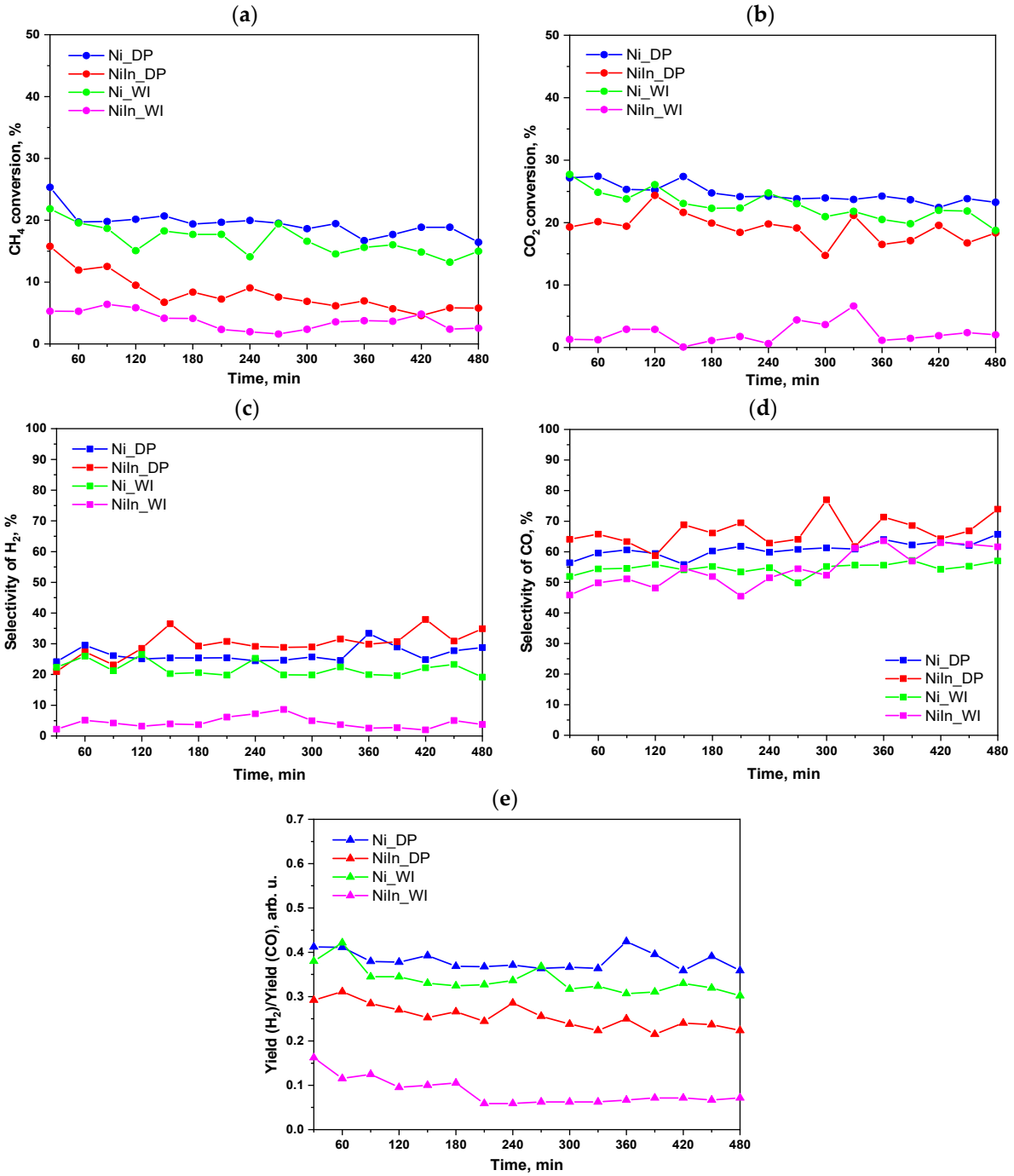

Figure 6. Conversion of (**a**) CH_4 and (**b**) CO_2, selectivity for (**c**) H_2 and (**d**) CO and (**e**) yield ratio of the products for the catalysts investigated (The thermodynamic equilibrium conversion values are 56% for CH_4 and 68% for CO_2, while the corresponding H_2/CO ratio is 0.8).

Table 4. Determination of the carbon content of the catalysts under investigation before and after the DRM reaction.

Sample	C before	C after
	wt.%	
Ni_WI	0.4	0.5
NiIn_WI	0.3	0.5
Ni_DP	0.4	5.3
NiIn_DP	0.5	1.0

In Figure S9a, which shows the TEM images and elemental maps of the Ni_DP catalyst sample used in the DRM reaction, we can observe multi-walled carbon nanotubes with lengths of several hundred nm and outer diameters of 10–18 nm. In addition, no deposited carbon could be found on the surfaces of the spent NiIn_DP, Ni_WI and NiIn_WI catalysts according to TEM studies (Figures S9b and S10a,b). Figure S8b shows a TGA curve obtained over the spent Ni_DP sample reflecting, in a single main peak, the oxidation of amorphous carbon below 350–400 °C and that of the graphitic nanotubes at a surprisingly low temperature of 450–550 °C. This low temperature shows the positive contribution of ceria to the removal of coke.

The results of the DRM catalytic tests (Figures 6 and S7) show that the activity of the investigated monometallic catalysts practically does not decrease as a function of time on the stream. The rather small, if any, decrease might be due to the migration, agglomeration and faceting of Ni particles at a high reaction temperature during a 6 h TOS. In fact, it can be seen in Figure S9a that the Ni particles in the spent Ni_DP sample are more developed than in the fresh state, and the very small particles have become fewer, while the relative number of larger particles increased up to a size of about 12 nm. The Ni(In) particle sizes of the spent NiIn_DP catalyst (Figure S9b) seemed to be more enlarged compared the fresh catalyst. The spent Ni_WI catalyst showed uniformly distributed metallic particles with diameters up to 15 nm, while the Ni in the bimetallic NiIn_WI sample is the least dispersed among the spent catalysts and exhibits particles in the size range of 6–40 nm, as visible in Figure S10. However, note that these particle sizes are only estimations and cannot be considered as representative average size data. The Ni/In atomic ratios over the entire measured area shown in Figures S9b and S10b are 31 and 28, respectively (close to the nominal bulk value, 24), but the more precise distribution of In cannot be investigated due to the low In signals in smaller areas.

Concerning the indium effect with respect to coking, we can point out that a surprisingly low amount of indium is enough but must be located at optimal places on the nickel surface to not fully quench the catalytic activity but just decrease the CH_4 dissociation tendency to a certain level. At a given low In loading (Ni >> In), the nickel dispersion, the interaction of Ni and In (and the support) and also the type of alloy (surface or bulk) are all influenced by the preparation method and govern the final catalytic property. In the case of unreducible oxide-supported Ni catalysts, indium seems to have a stronger or more beneficial promoter effect than on ceria support. The study of the allocation of indium under reaction conditions would require highly sophisticated surface science techniques, but DRIFTS at our disposal can help a lot.

To minimize the extent of migration and agglomeration of Ni and NiIn ensembles on the catalyst surface during the DRM reaction and thus prolong the catalyst performance, catalyst formulations deposited on supports that have a higher internal porosity and thermal stability compared to the ceria-based catalysts employed in the present study should be used [32,33]. In order to carry out the DRM reaction with a negligible accumulation of carbonaceous deposits on the catalyst surface, the CH_4 and CO_2 activation processes must be kinetically balanced. The results presented above show that this can be achieved, for example, in two ways: (i) by reducing the activity of very small Ni particles (such as those present on the surface of the Ni_DP catalyst) by dilution with In (or another transition

metal such as Co or Cu [34,35]) or (ii) by synthesizing a catalyst with an appropriate size of Ni particles in a real intimate contact with ceria inside the support pores (as in the present study in the case of the Ni_WI catalyst).

3. Experimental Section

3.1. Catalyst Preparation

Monometallic Ni/CeO_2 catalysts with a Ni loading of 3.0 wt.% and bimetallic $NiIn/CeO_2$ samples with the same Ni concentration and an In concentration of 0.25 wt.% (molar ratio Ni/In = 24) were prepared using both deposition–precipitation (DP) and wet impregnation (WI). The resulting samples are referred to as Ni_DP, NiIn_DP, Ni_WI and NiIn_WI. Commercially available CeO_2 nanopowder (Aldrich, WY, USA), $Ni(NO_3)_2$ (Aldrich) and $InCl_3 \times 4H_2O$ (Aldrich) were used as support materials or precursors, high purity water as a solvent and urea as a precipitant. In the preparation of DP-based samples, 1.5 g of cerium oxide and 2.5 g of urea were suspended in 155 mL of ultrapure water and stirred at room temperature until the urea dissolved. Then, a corresponding volume of 0.2 M $Ni(NO_3)_2$ was added, and for the NiIn_DP catalyst, 0.06 M $InCl_3$ solution was also added. Then, the temperature was increased to 90 °C with a ramp of 10 °C/min, and the mixture was stirred for 3 h (final pH ~ 8.5). After cooling to room temperature, the sample was subjected to 3 cycles of centrifugation and washing steps. For the WI-based materials, 1.5 g of ceria was suspended in 3.96 mL of 0.2 M $Ni(NO_3)_2$ or in a mixture of 3.96 mL of 0.2 M $Ni(NO_3)_2$ and 0.55 mL of 0.06 M $InCl_3$ solutions. The dense suspensions were stirred at room temperature for 1 h and at 60 °C for another 1.5 h, during which time the solvent was evaporated. All catalyst samples were dried in an oven at 80 °C for one day and then calcined in air at 650 °C for 2 h.

3.2. Surface and Textural Characterizations

The porosity of the prepared catalysts in their calcined state was determined by nitrogen adsorption/desorption experiments carried out at −196.15 °C using a TriStar II 3020 instrument (Micromeritics, Norcross, GA, USA). Prior to the measurements, the samples were degassed in a nitrogen stream (Messer, Ruše, Slovenia, purity 6.0) at 90 °C for 60 min and at 180 °C for 240 min. The specific surface area (S_{BET}) and pore size distribution were determined according to the Brunauer–Emmett–Teller (BET) theory and the theory of Barret, Joyner and Halenda (BJH).

The structural properties and compositions of all investigated calcined catalysts were characterized using a PANalytical X'Pert PRO MPD X-ray diffractometer (Almero, The Netherlands) (Cu Kα1 = 0.154 nm). The scanning range was from 10 to 90° with an increment of 0.034°. The PDFs of the standards were obtained from the International Center for Diffraction Data (ICDD).

The reducibility of the calcined samples and also the calcined pure support was investigated using TPR in an AutoChem II 2920 instrument (Micromeritics, Norcross, GA, USA) equipped with a thermal conductivity detector (TCD). The resulting H_2O was frozen with a cold trap prior to the analysis. The samples (50 mg) were pretreated in situ in 10% O_2/He (30 mL/min) at 350 °C for 30 min. After cooling in argon, the temperature was raised to 650 °C in a 10% H_2/Ar stream (30 mL/min) at a heating rate of 10 °C/min, followed by an isothermal phase of 1 h.

The surface compositions of the samples were determined using a KRATOS XSAM 800 XPS instrument (Manchester, UK). The samples were analyzed by using an unmonochromatized Al K-alpha source (1486.6 eV). All measurements were conducted in the fixed analyzer transmission (FAT) mode. On each sample, wide-range spectra were collected at an analyzer pass energy of 80 eV to survey the elemental composition. The pass energy of the hemispherical analyzer was set at 40 eV for recording the high-resolution spectra of the Ce 3d, Ni 2p, O 1s and C 1s regions. The u‴ component of the Ce 3d peak at 916.7 eV was used as reference for charge compensation. The ex situ calcined samples were measured after an in situ reduction at 650 °C for 1 h in H_2 using the instrument's atmospheric

pretreatment chamber. The ratio of the elements at the surface was calculated from the integral intensities of the XPS lines using sensitivity factors given by the manufacturer. For the evaluation of the Ce^{3+} amount, the data treatment method of Pardo et al. [36] was used.

The morphology of the catalysts in the reduced state (after the TPR measurements) and after the DRM tests was examined using a Thermo Fisher (Waltham, MA, USA) Titan Themis 200 kV transmission electron microscope with corrected spherical aberration (Cs) and 0.09 nm HRTEM and 0.16 nm STEM. STEM-EDS with the 4 Thermo Fischer (Waltham, USA) "Super X G1" EDS detectors built into the microscope was applied to determine the distribution and concentrations of catalyst components in the selected areas. The data were analyzed, and elemental maps of Ni, In and Ce were generated by background correction and adjustment of the Ni-K, In-L and Ce-L intensities using Velox 3.12.1 software.

The chemical compositions and morphologies of the synthesized materials were investigated using a Carl Zeiss field emission scanning electron microscope (model FE-SEM SUPRA 35 VP, Oberkochen, Germany) equipped with an Oxford Instruments dispersive energy detector (model Inca 400, Abringdon, Oxfordshire, UK).

3.3. Diffuse Reflectance Infrared Fourier Transform Spectroscopy (DRIFTS)

The catalysts and the pure support reduced in the TPR measurements were characterized by CO adsorption followed by DRIFT spectroscopy using a Nicolet iS50 infrared spectrometer equipped with an MCT-A detector and a Harrick DRIFTS accessory (Pleasantville (NY), USA) with an environmental chamber that could be heated to 900 °C. Approximately 20 mg of the sample powder was placed in the sample holder and pretreated in situ at 500 °C (heating rate 10 °C/min) in a 5% H_2/Ar stream for 30 min. After cooling to room temperature in the same gas mixture, the sample was exposed to a 1% CO/Ar stream for 5 min, followed by a 5 min rinse of the cell with 5% H_2/Ar. A temperature-programmed surface reaction (TPSR) of the adsorbed CO was then performed in a 5% H_2/Ar stream up to 300 °C. After the removal of all adsorbed CO, 1% CO/Ar was added for 5 min, followed by another 5% H_2/Ar purge at the same temperature. The spectra were recorded by collecting 64 scans with a resolution of 4 cm^{-1} at room temperature and 300 °C in the presence of CO as well as after the 5% H_2/Ar purge and during the temperature rise to 300 °C at 25 °C intervals. The log(1/R) spectra shown (R is the reflectivity) were corrected by a background spectrum recorded immediately before CO uptake or by spectra measured at similar temperatures during cooling after the in situ reduction pretreatment.

3.4. Catalytic Experiments

The experiments on the dry reforming of methane were carried out in a quartz tube fixed-bed reactor in the computer-controlled Microactivity Reference reactor system (PID Eng&Tech, Madrid, Spain). For the reaction, the calcined catalyst (25 mg) was diluted with SiC (75 mg) and placed on a quartz wool flake in the reactor. The catalyst was then heated in nitrogen from room temperature to 200 °C and then reduced at 650 °C in pure hydrogen for 1 h. The reactor was then purged with nitrogen at 650 °C for 30 min, after which the reaction was carried out at 650 °C for 8 h. The gas feed stream was a 1:1 mixture of CO_2 and CH_4 at a flow rate of 70 mL/min. Samples of the product mixture were taken every 30 min during each experiment and analyzed using an Agilent 7890A (Santa Clara, CA, USA) online chromatograph equipped with Porapak Q, HayeSep Q and Molecular Sieve 5A columns (all from Agilent) and two TCD detectors. The reactant conversion, product selectivity and yield and carbon balance were calculated using the following Equations (1)–(7):

$$X_{CO_2} = \frac{f(CO_2, \text{in}) - f(CO_2, \text{out})}{f(CO_2, \text{in})} \times 100\% \quad (1)$$

$$X_{CH_4} = \frac{f(CH_4, \text{in}) - f(CH_4, \text{out})}{f(CH_4, \text{in})} \times 100\% \quad (2)$$

$$S_{H_2} = \frac{f(H_2, \text{out})}{2(f(CH_4, \text{in}) - f(CH_4, \text{out}))} \times 100\% \quad (3)$$

$$S_{CO} = \frac{f(CO, \text{out})}{f(CH_4 + CO_2, \text{in}) - f(CH_4 + CO_2, \text{out})} \times 100\% \quad (4)$$

$$Y_{H_2} = \frac{f(H_2, \text{out})}{2f(CH_4, \text{in})} \times 100\% \quad (5)$$

$$Y_{CO} = \frac{f(CO, \text{out})}{f(CH_4, \text{in}) + f(CO_2, \text{in})} \times 100\% \quad (6)$$

$$C_{\text{balance}} = \frac{f(CH_4, \text{out}) + f(CO_2, \text{out}) + f(CO, \text{out})}{f(CH_4, \text{in}) + f(CO_2, \text{in})} \quad (7)$$

where f is the volumetric flow rate of each component in mL/min.

A Perkin Elmer CHNS 2400 Series II analyzer (Waltham, MA, USA) was used to determine the extent of carbon deposition on the catalyst surface after the DRM reaction. Using a Perkin Elmer Pyris1 TGA instrument (Waltham, MA, USA), we performed a TGA in air (50 mL/min) to determine the nature of potential coke formation.

4. Conclusions

In the present study, the surface and textural analyses, a comprehensive CO-DRIFTS investigation and the catalytic performances of Ni/CeO_2 and $NiIn/CeO_2$ catalysts prepared using two different methods (wet impregnation (WI) and deposition–precipitation (DP)) were investigated.

The nitrogen adsorption–desorption isotherms showed that the addition of Ni and the high temperature calcination significantly decreased the specific surface area of the impregnated samples, probably due to ceria sintering and the blocking of pores. The minimal addition of In further decreased the specific surface area and pore volume. XRD analysis showed that Ni and In were deposited on CeO_2 with some lattice incorporation detectable only in the case of the monometallic DP sample, which somewhat affected the crystallinity. The H_2-TPR profiles showed clear changes in the interactions upon the addition of In to Ni only for the WI method. STEM-EDS-derived elemental maps suggested the formation of slightly smaller Ni and much smaller NiIn particles on the CeO_2 support using the DP method compared to the WI technique. XPS detected higher nickel and indium concentrations for the DP samples, proving the surface location and the higher dispersion of metals in this case. Ceria reducibility (amount of Ce^{3+}) was not significant and lower than 10% in all cases. The CO-DRIFTS analysis demonstrated that there was a direct interaction between Ni and In in the bimetallic samples due to the electronic interference of Ni by In, because some dilution of the Ni surface by In occurred, resulting in the formation of a NiIn (surface) alloy. In the DRM reaction, the Ni/CeO_2 catalysts showed a similar activity, which was higher than that of their bimetallic counterparts. The Ni_DP catalyst exhibited considerable coking of the catalyst surface, which was significantly reduced by the addition of In. The STEM-EDS studies indicated some agglomeration and faceting of Ni and/or NiIn particles during the DRM reaction, which somewhat affected the performance of the catalysts.

In summary, the study highlights the complex interplay between the catalyst preparation methods, metal additives, surface properties and catalytic performance in the DRM reaction and emphasizes the role of the addition of In to the Ni particles to reduce the carbon formation by kinetically balancing the activation processes of CH_4 and CO_2. Further work is proposed to optimize the addition of In to supported Ni catalysts that enable improved thermal stability.

Supplementary Materials: The following supporting information can be downloaded at: https://www.mdpi.com/article/10.3390/catal14060383/s1, Figure S1: (a) Nitrogen adsorption–desorption isotherms, (b) pore-size distribution and (c) XRD diffractograms of the studied catalysts in the

calcined state. The dotted lines in the diffractograms represent the standard diffractions for PDF ICDD 04-015-0377, 01-080-6915 and 04-0102-0220 of cubic CeO_2; Figure S2: Comparison of TEM images and elemental maps of Ni and In for fresh (a) Ni_DP and (b) NiIn_DP catalyst samples; Figure S3: Comparison of TEM images and elemental maps of Ni and In for fresh (a) Ni_WI and (b) NiIn_WI catalyst samples; Figure S4: SEM-EDS mapping images of Ni_WI, NiIn_WI, Ni_DP and NiIn_DP samples; Figure S5: XPS spectra of the in situ reduced Ni_DP (red), NiIn_DP (black), Ni_WI (blue) and NiIn_WI (green) catalysts in the Ni $2p_{3/2}$ and Ni LMM region and the In 3d region for the bimetallic catalysts; Figure S6: Difference spectra of DRIFT spectra recorded at room temperature after CO adsorption followed by 5 min of purging with 5% H_2/Ar (red curves in Figure 4) minus those previously recorded in 1% CO/Ar after 5 min of exposure (dashed curves in Figure 4) on the catalyst samples; Figure S7: Yields of (a) H_2 and (b) CO obtained using DRM of the catalysts under study, reduced at 650 °C; Figure S8: Graphical representation of the (a) carbon balance of the catalysts studied and (b) TGA of the spent Ni_DP catalyst conducted in air; Figure S9: TEM images (left) and elemental maps (right) of spent (a) Ni_DP and (b) NiIn_DP catalysts. The Ni/In atomic ratio on the measured area of NiIn_DP sample is 31; Figure S10: TEM images (left) and elemental maps (right) of spent (a) Ni_WI, (b) and NiIn_WI catalysts. The Ni/In atomic ratio on the measured area of the NiIn_WI sample is 28; Table S1: Experimental values of cell unit obtained from XRD measurements (Figure S1c) and corresponding cell volume; Table S2: Results of SEM-EDS elemental analysis of the studied materials.

Author Contributions: Conceptualization, A.H. and A.P.; Methodology, A.B.; Validation, A.H.; Investigation, A.H., A.B., M.N., G.S., M.R. and G.Ž.; Resources, A.H. and A.P.; Writing—original draft, A.H., A.B., M.R. and G.Ž.; Writing—review & editing, A.H. and A.P.; Visualization, A.B., M.N., G.S., M.R. and G.Ž.; Supervision, A.P.; Project administration, A.H.; Funding acquisition, A.H. and A.P. All authors have read and agreed to the published version of the manuscript.

Funding: The authors acknowledge the financial support from the Slovenian Research and Innovation Agency (research core funding no. P2-0150) and the National Research, Development and Innovation Office for researcher mobility (no. 2019-2.1.11-TÉT-2020-00188).

Data Availability Statement: The raw data supporting the conclusions of this article will be made available by the authors on request.

Conflicts of Interest: The authors declare no conflicts of interest.

References

1. Lin, T.-Y.; Chiu, Y.-H.; Lin, Y.-N.; Chang, T.-H.; Lin, P.-Y. Greenhouse gas emission indicators, energy consumption efficiency, and optimal carbon emission allowance allocation of the EU countries in 2030. *Gas Sci. Eng.* **2023**, *110*, 204902. [CrossRef]
2. Yusuf, M.; Farooqi, A.S.; Alam, M.A.; Keong, L.K.; Hellgardt, K.; Abdullah, B. Performance of Ni/Al_2O_3-MgO catalyst for Dry Reforming of Methane: Effect of preparation routes. *IOP Conf. Ser. Mater. Sci. Eng.* **2021**, *1092*, 012069. [CrossRef]
3. United Nations Environment Programme, Emissions Gap Report 2022: The Closing Window—Climate Crisis Calls for Rapid Transformation of Societies. Nairobi. Available online: https://www.unep.org/emissions-gap-report-2022 (accessed on 10 May 2024).
4. Dyonisius, M.N.; Petrenko, V.V.; Smith, A.M.; Hua, Q.; Yang, B.; Schmitt, J.; Beck, J.; Seth, B.; Bock, M.; Hmiel, B.; et al. Old carbon reservoirs were not important in the deglacial methane budget. *Science* **2020**, *367*, 907–910. [CrossRef]
5. Sharifianjazi, F.; Esmaeilkhanian, A.; Bazli, L.; Eskandarinezhad, S.; Khaksar, S.; Shafiee, P.; Yusuf, M.; Abdullah, B.; Salahshour, P.; Sadeghi, F. A review on recent advances in dry reforming of methane over Ni- and Co-based nanocatalysts. *Int. J. Hydrogen Energy* **2022**, *47*, 42213–42233. [CrossRef]
6. Mao, Y.; Zhang, L.; Zheng, X.; Liu, W.; Cao, Z.; Peng, H. Coke-resistance over Rh–Ni bimetallic catalyst for low temperature dry reforming of methane. *Int. J. Hydrogen Energy* **2023**, *48*, 13890–13901. [CrossRef]
7. Károlyi, J.; Németh, M.; Evangelisti, C.; Sáfrán, G.; Schay, Z.; Horváth, A.; Somodi, F. Carbon dioxide reforming of methane over Ni–In/SiO_2 catalyst without coke formation. *J. Ind. Eng. Chem.* **2018**, *58*, 189–201. [CrossRef]
8. Németh, M.; Sáfrán, G.; Horváth, A.; Somodi, F. Hindered methane decomposition on a coke-resistant Ni-In/SiO_2 dry reforming catalyst. *Catal. Commun.* **2019**, *118*, 56–59. [CrossRef]
9. Németh, M.; Somodi, F.; Horváth, A. Interaction between CO and a Coke-Resistant NiIn/SiO_2 Methane Dry Reforming Catalyst: A DRIFTS and CO Pulse Study. *J. Phys. Chem. C* **2019**, *123*, 27509–27518. [CrossRef]
10. Horváth, A.; Németh, M.; Beck, A.; Marőti, B.; Sáfrán, G.; Pantaleo, G.; Liotta, L.F.; Venezia, A.M.; La Parola, V. Strong impact of indium promoter on Ni/Al_2O_3 and Ni/CeO_2-Al_2O_3 catalysts used in dry reforming of methane. *Appl. Catal. A* **2021**, *621*, 118174. [CrossRef]

11. Horváth, A.; Németh, M.; Beck, A.; Sáfrán, G.; La Parola, V.; Liotta, L.F.; Žerjav, G.; Roškarič, M.; Pintar, A. Longevity increase of an impregnated Ni/CeO_2-Al_2O_3 dry reforming catalyst by indium. *Appl. Catal. A* **2024**, *669*, 119495. [CrossRef]
12. El-Habib, A.; Addou, M.; Aouni, A.; Diani, M.; Nouneh, K.; Zimou, J.; Marjaoui, A.; Barbouch, Z.; Zanouni, M.; El Jouad, Z. Effect of indium doping on the structural. optical and electrochemical behaviors of CeO_2 nanocrystalline thin films. *Opt. Mater.* **2022**, *127*, 112312. [CrossRef]
13. Sharma, S.K.; Paul, B.; Pal, R.S.; Bhanja, P.; Banerjee, A.; Samanta, C.; Bal, R. Influence of Indium as a Promoter on the Stability and Selectivity of the Nanocrystalline Cu/CeO_2 Catalyst for CO_2 Hydrogenation to Methanol. *ACS Appl. Mater. Interfaces* **2021**, *13*, 28201–28213. [CrossRef]
14. Thommes, M.; Kaneko, K.; Neimark, A.V.; Olivier, J.P.; Rodriguez-Reinoso, F.; Rouquerol, J.; Sing, K.S.W. Physisorption of gases, with special reference to the evaluation of surface area and pore size distribution (IUPAC Technical report). *Pure Appl. Chem.* **2015**, *87*, 1051–1069. [CrossRef]
15. Khobragade, R.; Roškarič, M.; Žerjav, G.; Košiček, M.; Zavašnik, J.; Van de Velde, N.; Jerman, I.; Tušar, N.N.; Pintar, A. Exploring the effect of morphology and surface properties of nanoshaped Pd/CeO_2 catalysts on CO_2 hydrogenation to methanol. *Appl. Catal. A* **2021**, *627*, 118394. [CrossRef]
16. Naidu, B.N.; Kumar, K.D.P.L.; Saini, H.; Kumar, M.; Kumar, T.N.; Prasad, V.V.D.N. Coke deposition over Ni-based catalysts for dry reforming of methane: Effects of MgO-Al_2O_3 support and ceria, lanthana promoters. *J. Environ. Chem. Eng.* **2022**, *10*, 106980. [CrossRef]
17. Wang, Y.; Hu, Q.; Wang, X.; Huang, Y.; Wang, Y.; Wang, F. Ni/CeO_2 Catalyst Prepared via Microimpinging Stream Reactor with High Catalytic Performance for CO_2 Dry Reforming Methane. *Catalysts* **2022**, *12*, 606. [CrossRef]
18. Li, M.; Pham, T.H.M.; Ko, Y.; Zhao, K.; Zhong, L.; Luo, W.; Züttel, A. Support-Dependent Cu–In Bimetallic Catalysts for Tailoring the Activity of Reverse Water Gas Shift Reaction. *ACS Sustain. Chem. Eng.* **2022**, *10*, 1524–1535. [CrossRef]
19. Wang, L.; Liu, Y. Highly Active and Selective Nickel–Cerium(IV) Oxide Catalyst for Water–Gas Shift Reaction. *Chem. Lett.* **2008**, *37*, 74–75. [CrossRef]
20. Wang, L.; Zhang, S.; Liu, Y. Reverse water gas shift reaction over Co-precipitated Ni-CeO_2 catalysts. *J. Rare Earths* **2008**, *26*, 66–70. [CrossRef]
21. Ni, Z.; Djitcheu, X.; Gao, X.; Wang, J.; Liu, H.; Zhang, Q. Effect of preparation methods of CeO_2 on the properties and performance of Ni/CeO_2 in CO_2 reforming of CH_4. *Sci. Rep.* **2022**, *12*, 5344. [CrossRef]
22. Li, L.; Jiang, B.; Tang, D.; Zheng, Z.; Zhao, C. Hydrogen Production from Chemical Looping Reforming of Ethanol Using Ni/CeO_2 Nanorod Oxygen Carrier. *Catalysts* **2018**, *8*, 257. [CrossRef]
23. Liu, X.; Zuo, Y.; Li, L.; Huang, X.; Li, G. Heterosturcture NiO/$Ce_{1-x}Ni_xO_2$: Synthesis and synergistic effect of simultaneous surface modification and internal doping for superior catalytic performance. *RSC Adv.* **2014**, *4*, 6397–6406. [CrossRef]
24. Crist, B.V. *Handbook of Monochromatic XPS Spectra—The Elements and Native Oxides*; John Wiley & Sons: Chichester, UK, 2000; Volume 1, p. 133.
25. Agnelli, M.; Swaan, H.M.; Marquez-Alvarez, C.; Martin, G.A.; Mirodatos, C. CO Hydrogenation on a Nickel Catalyst: II. A Mechanistic Study by Transient Kinetics and Infrared Spectroscopy. *J. Catal.* **1998**, *175*, 117–128. [CrossRef]
26. Blackmond, D.G.; Ko, E.I. Structural Sensitivity of CO Adsorption and H_2/CO Coadsorption on Ni/SiO_2 Catalysts. *J. Catal.* **1985**, *96*, 210–221. [CrossRef]
27. Mihaylov, M.; Lagunov, O.; Ivanova, E.; Hadjiivanov, K. Determination of Polycarbonyl Species on Nickel-Containing Catalysts by Adsorption of CO Isotopic Mixtures. *Top. Catal.* **2011**, *54*, 308–317. [CrossRef]
28. Mihaylov, M.; Hadjiivanov, K.; Knözinger, H. Formation of $Ni(CO)_4$ during the Interaction between CO and Silica-Supported Nickel Catalyst: An FTIR Spectroscopic Study. *Catal. Lett.* **2001**, *76*, 59–63. [CrossRef]
29. Wendlandt, K.-P.; Bremer, H.; Vogt, F.; Reschetilowski, W.P.; Mörke, W.; Hobert, H.; Weber, M.; Becker, K. Metal Carrier Interactions in Zeolite Y Catalysts Containing Nickel. *Appl. Catal.* **1987**, *31*, 65–72. [CrossRef]
30. Rao, K.M.; Spoto, G.; Zecchina, A. IR Investigation of $Ni(CO)_4$ Interaction with Silicalite, ZSM-5, Zeolite-Y, and γ-Al_2O_3. *Langmuir* **1989**, *5*, 319–325.
31. Andersson, M.P.; Abild-Pedersen, F.; Remediakis, I.N.; Bligaard, T.; Jones, G.; Engbæk, J.; Lytken, O.; Horch, S.; Nielsen, J.H.; Sehested, J.; et al. Structure Sensitivity of the Methanation Reaction: H_2-Induced CO Dissociation on Nickel Surfaces. *J. Catal.* **2008**, *255*, 6–19. [CrossRef]
32. Aw, M.S.; Zorko, M.; Djinović, P.; Pintar, A. Insights into durable NiCo catalysts on β-SiC/$CeZrO_2$ and γ-Al_2O_3/$CeZrO_2$ advanced supports prepared from facile methods for CH_4–CO_2 dry reforming. *Appl. Catal. B* **2015**, *164*, 100–112. [CrossRef]
33. Aw, M.S.; Dražić, G.; Djinović, P.; Pintar, A. Transition metal pairs on ceria-promoted, ordered mesoporous alumina as catalysts for the CO_2 reforming reaction of methane. *Catal. Sci. Technol.* **2016**, *6*, 3797–3805. [CrossRef]
34. Djinović, P.; Pintar, A. Stable and selective syngas production from dry CH_4-CO_2 streams over supported bimetallic transition metal catalysts. *Appl. Catal. B* **2017**, *206*, 675–682. [CrossRef]

35. Lee, J.; Bae, Y.; Hong, K.; Hong, J. Comparative evaluation of Ni-based bimetallic catalysts for dry reforming of methane at low temperature: The effect of alloy itself on performance. *Int. J. Energy Res.* **2022**, *46*, 11228–11249. [CrossRef]
36. Pardo, A.; Feliú, S.; Merino, M.C.; Arrabal, R.; Matykina, E. The effect of cerium and lanthanum surface treatments on early stages of oxidation of A361 aluminium alloy at high temperature. *Appl. Surf. Sci.* **2007**, *254*, 586–595. [CrossRef]